FINAL TECHNICAL REPORT

IPC "Two-Color" Analysis of X-Ray Galaxy Clusters

PI: Raymond E. White III

Department of Physics and Astronomy
University of Alabama
Tuscaloosa, AL 35487-0324

NASA ADP Grant: NAG 5 1188

8/1/89—1/31/90

IPC "Two-Color" Analysis of X-Ray Galaxy Clusters

Background

I have determined the mass distributions of several clusters of galaxies by using X-ray surface brightness data from the *Einstein Observatory* Imaging Proportional Counter (IPC). Determining cluster mass distributions is important for constraining the nature of the dark matter which dominates the mass of galaxies, galaxy clusters and the Universe. Galaxy clusters are permeated with hot gas in hydrostatic equilibrium with the gravitational potentials of the clusters. Cluster mass distributions can be determined from X-ray observations of cluster gas by using the equation of hydrostatic equilibrium and knowledge of the density and temperature structure of the gas:

$$M(r) = \frac{k}{\mu m G}\left(\frac{d\ln\rho}{d\ln r} + \frac{d\ln \mathrm{T}}{d\ln r}\right) T(r) r. \qquad (1)$$

Here M is the total mass within radius r from the cluster center, ρ and T are the gas density and temperature, and k, μm and G are the Boltzmann constant, mean mass per gas particle and the gravitational constant, respectively. Note that the logarithmic derivatives of ρ and T in this equation are simply the respective local slopes of density and temperature profiles.

The X-ray surface brightness at some distance r from the cluster is the result of the volume X-ray emissivity being integrated along the line-of-sight in the cluster. The X-ray surface brightness profile $S_x(r)$ can be deprojected to give the local volume emissivity $\epsilon_x(r) = \rho^2(r)\Lambda_x(T(r))$, which is a function of the local gas density and the radiative cooling function $\Lambda_x(T)$ (the latter of which has been convolved with the spectral response of the detector). Because the spectral response of the *Einstein Observatory* IPC was rather insensitive to temperature variations, accurate gas density profiles can be extracted from such deprojected volume emissivities: that is, $\Lambda_x(T)$ is fairly constant for the bulk of the temperature range expected in clusters. Thus, the slope of the density profile and its contribution to the total mass determination in equation (1) is well-constrained by the high spatial resolution surface brightness profiles provided by the IPC. However, the poor spectral resolution of the IPC has prevented temperature profiles $T(r)$ from being extracted with similar accuracy.

Analysis

To estimate the temperature structure of the hot gas in several galaxy clusters, I divide IPC surface brightness data into two different energy bands: 0.56-1.5 keV and 1.5-3.5 keV. Only two broad bands are chosen in order to maximize the counts in each band, reducing their statistical uncertainty. Although the *Einstein* IPC was sensitive to photons softer than 0.56 keV, they were excluded from consideration because they are most subject to uncertainties in the column density of intervening X-ray-absorbing matter.

Volume X-ray emissivities are extracted from the surface brightness profiles, after background subtraction and vignetting correction. A ratio of emissivities in the two energy

bands provides a temperature estimate when compared to theoretical emissivity ratios for these two bands. Theoretical emissivity ratios are derived from the XSPEC software (Shafer, Arnaud, Haberl, Tennant 1990), which can convolve thermal spectra with the spectral response of the IPC. The photon statistics remain poor, nonetheless, so there is a considerable tradeoff to be made: 1) one can derive reasonably well-constrained temperatures at very few (maybe only one) positions, leading to no or very coarse mass profiles; or 2) one can try to retain high spatial resolution, but lose accuracy in the temperature profile, leading to poorly determined mass profiles.

I first tried to derive reasonably smooth mass profiles by retaining considerable spatial resolution with a Monte Carlo approach to the data analysis. Synthetic surface brightness data were generated from the original data by assuming Poisson errors. Smooth fits were made to the resulting synthesized surface brightness profiles in each energy band. The chosen forms of the surface brightness fits allowed emissivity profiles to be deduced analytically. The subsequent ratio of the emissivity profiles in the two energy bands allowed smooth temperature profiles, and therefore smooth mass profiles, to be deduced. Errors were estimated from the dispersion in the temperature and mass profiles after 20-100 realizations of the surface brightness data were processed.

Initial analysis of the X-ray data for clusters A496 and A2199 seemed promising, in that smooth and reasonable mass profiles were derived from fits to the raw data. However, the subsequent Monte Carlo synthesis and error analysis showed that the uncertainties in the derived temperature and mass profiles were so large that the temperature and mass profiles could not be interestingly constrained.

I then turned to a straightforward, non-synthetic analysis of the data in order to determine the maximum spatial resolution for which I could still obtain reasonably constrained temperatures. I started by combining all of the data in one spatial bin (resulting in no spatial resolution) in order to derive the most accurate temperature. I then deprojected the data into successively smaller spatial bins until the temperature uncertainty in each bin grew to make the temperature estimates uninteresting.

The deprojection routine I developed to extract volume emissivities from surface brightness data also calculates the errors in the emissivities so derived. Temperatures were derived from a comparison of the ratio of deprojected count emissivity in the two energy bands to theoretical ratios derived from XSPEC spectral synthesis. The metal abundances and column densities of intervening, X-ray absorbing matter were held fixed in deriving tables of temperature vs. hardness ratio. Abundances were taken from *Ginga* observations of Hatsukade (1989) or *EXOSAT* observations of Edge (1989). Column densities of intervening X-ray absorbing matter were taken from the same sources. I have been able to derive reasonably well-constrained temperatures for at least two and as many as four spatial bins in four clusters: A262, A1060, A2199 and A496. The temperature profiles for these clusters are shown in Figures $1a - d$. The temperatures are plotted against angular distance from the cluster centers. The spatial conversion (assuming $q_0 = 0.5$ and $H_0 = 50$ km/s/Mpc) for each cluster is indicated in the lower right of each panel.

The global temperatures I derive for A262 and A1060 are in excellent agreement with

temperatures derived from other spectroscopic instruments (see Table 1). However, the temperatures of A496 and A2199 are respectively hotter and cooler than those derived from other instruments (see Table 1). These systematic differences are probably due to the fact that I am deriving a temperature from only one hardness ratio, rather than from fits to the the full complement of energy resolution elements of the IPC. Nonetheless, even in the two clusters which have systematic temperature differences, I can still accurately assess the *isothermality* of their cluster atmospheres. If the clusters are isothermal to the outermost radii investigated, a systematic offset in the absolute temperature calibration cannot prevent that from being determined. However, if temperature structure exists, the actual shape cannot be accurately deduced without knowing whether the systematic errors in the derived temperatures are temperature-dependent. A262 and A1060 (see Figs. $1a, b$) appear to have roughly isothermal temperature profiles outside a cooler central bin. A496 also seems to be isothermal, but only two spatial bins proved feasible. A2199 seems to have a substantial temperature peak at intermediate radii. The cooler centers of A262 and A1060 are a signature of cooling flows and are also reflected in the fact that the central cooling times in these clusters is less than 10^{10} yrs (see Fig. 4).

I derived gas densities from the deprojected total emissivity (the full energy bandwidth of the prior two energy bands) using count-to-flux conversions derived from XSPEC modelling. I adopted the global temperatures derived above in determining the local gas density. The resulting distribution of gas mass are shown in Figures $2a, b$ for A262 and A1060, for which the global temperature determination proved accurate. Also shown in these figures are the total mass distributions I derive for A262 and A1060 using equation (1). I took the cluster gas to be isothermal at the derived global temperature (neglecting the temperature drop in the innermost region) and the slope of the density distribution was derived from the deprojected density profile. The gas mass to total mass ratio is shown in Figure 3, where it is clear that M_{gas}/M_{tot} rises outward to about 10% by ~500 kpc.

The cooling time distributions inferred from the local density and the (assumed constant) global temperature in A262 and A1060 are shown in Figure 4, where it is apparent that the cooling time is less than 10^{10} yrs in the central parts. This indicates that the central gas can radiate away its pressure support in a Hubble time, leading to a cooling flow. If the cooling flow is long-lived, the central temperature should be cooler, as is indicated in Figures $1a, b$.

These results, with some additional analysis, will be submitted to *The Astrophysical Journal* for publication.

The Energetics and Metal Abundances of Intracluster Gas

I was able to use some of the surface brightness data analyzed in the previously described investigation in an entirely different project, as well. I recently showed that various galaxy formation scenarios can be tested and distinguished by their relative impact on the physical state of intracluster gas. Intracluster gas gains a certain amount of energy in the course of galaxy cluster collapse. Additional energy may (or may not) be injected into intracluster gas through processes associated with galaxy formation before or during cluster collapse. If galaxy formation was truncated by galactic winds, then such winds would deposit metals

and energy into intracluster gas. Clusters with low velocity dispersions should be most affected by this additional energy deposition. If galaxies did not blow winds, then no such energy would be deposited. In the latter case, the high metal abundances observed in intracluster gas may be attributed to the stripping of metal-rich gas from galaxies, a process which does not add net energy to intracluster gas. Thus, these two galaxy formation scenarios can be distinguished by their relative impact on the energetics of intracluster gas.

If intracluster gas were energized solely by cluster collapse, then the gas should have the same specific energy (temperature) as the cluster mass and galaxies. The gas density should then have the same profile as the mass density if both are isothermal. In the galactic wind hypothesis, intracluster gas should have more specific energy than expected if the intracluster gas was energized solely by cluster collapse. Thus the gas temperature should exceed the kinetic temperature (velocity dispersion) of the galaxies, and the gas density profile should be shallower than the total mass density profile. A shallower gas density profile leads to a shallower X-ray surface brightness profile. These effects should be more pronounced for clusters with low velocity dispersions, because the depths of their potential wells are more comparable than those of high dispersion clusters to the depths of individual galaxies' potential wells. I showed that X-ray spectral observations of the gas in cool and hot clusters indicate that cool clusters have preferentially higher specific energy than the galaxies in such clusters. Furthermore, I showed that the surface brightness profiles of cool clusters tend to be shallower than those of hot clusters. To help fortify this latter point, I used some of the surface brightness data acquired and analyzed in the course of the previously described investigation of intracluster temperature profiles. Both the temperature and surface brightness observations are consistent with galaxies having blown energetically significant galactic winds in the past.

I presented these results at a meeting on "Superclusters and Clusters of Galaxies and Environmental Effects" held in July 1990 in Sesto, Italy. Reprints of the publication associated with this work ("The Metal Abundance and Specific Energy of Intracluster Gas," White, R. E. III 1991, *Astrophysical Journal*, **367**, 69-77) are included with this final report.

References

Edge, A. C. 1989, Ph.D. Thesis.
Hatsukade, I. 1989, Ph.D. Thesis, ISAS Research Note 435.
Shafer, R., Haberl, F., Arnaud, K. A., and Tennant, A. 1990, *XSPEC*.

Publications generated by this grant

"The Metal Abundance and Specific Energy of Intracluster Gas"
White, R. E. III 1991, *Astrophysical Journal*, **367**, 69-77.

"Temperature and Mass Profiles for Several Clusters of Galaxies"
White, R. E. III 1991, to be submitted to *Astrophys. J.*

Table 1

Cluster	Temperature (this study)	Temperature (other)	other Instrument
A 262	$1.86^{+0.37}_{-0.21}$	$2.42^{+0.31}_{-0.27}$	EXOSAT
A 1060	$2.53^{+0.22}_{-0.19}$	$2.55^{+0.04}_{-0.04}$	Ginga
A 496	$5.44^{+1.20}_{-0.85}$	$3.91^{+0.06}_{-0.06}$	Ginga
A 2199	$2.60^{+0.25}_{-0.20}$	$4.71^{+0.41}_{-0.35}$	EXOSAT

Temperatures in keV. Ginga temperatures from Hatsukade (1989); errors are 90% confidence. EXOSAT temperatures from Edge (1989); errors are 90% confidence. Temperature errors for this study are 1 sigma.

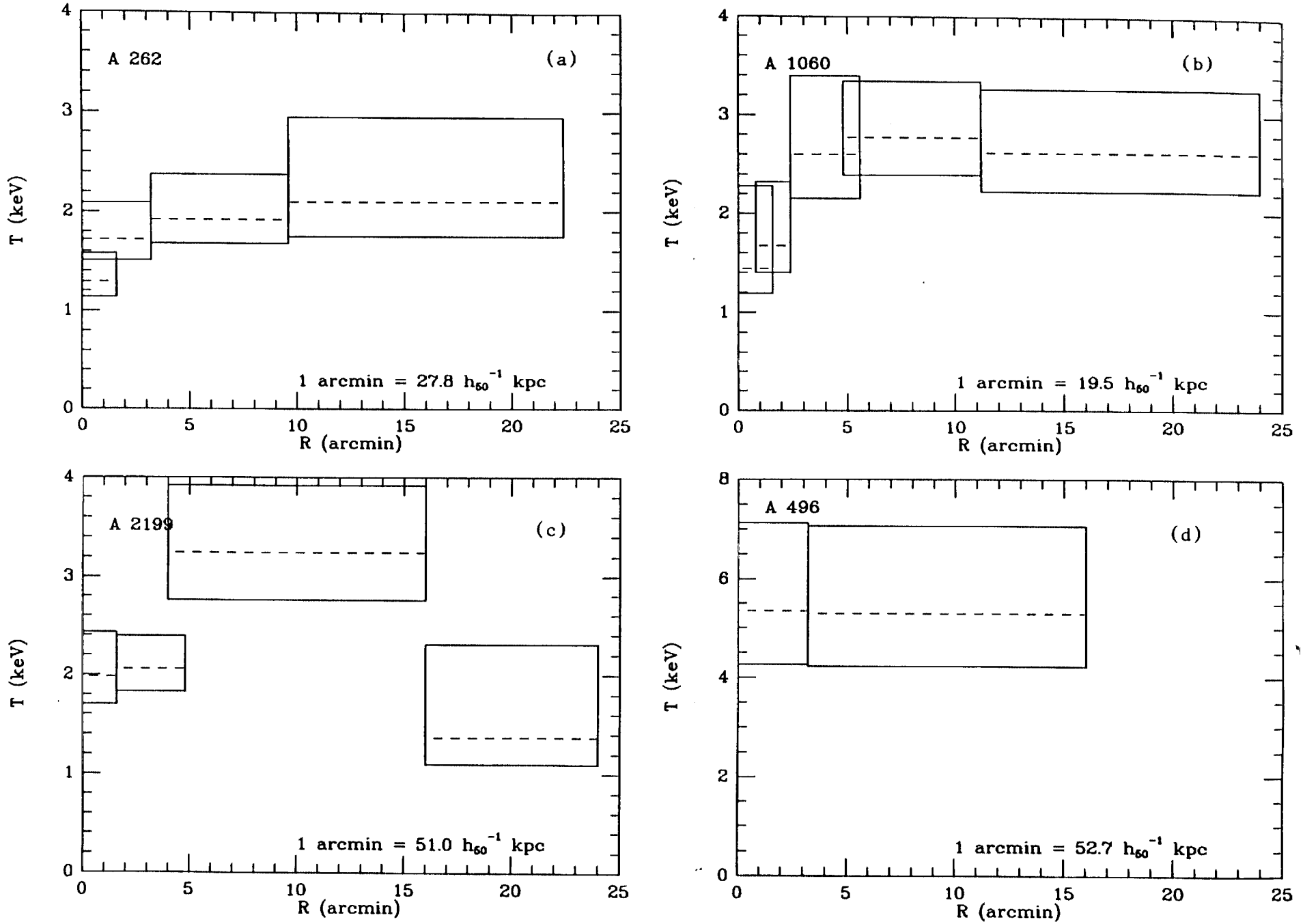
A 262
(a)
1 arcmin = 27.8 h_{50}^{-1} kpc
A 1060
(b)
1 arcmin = 19.5 h_{50}^{-1} kpc
A 2199
(c)
1 arcmin = 51.0 h_{50}^{-1} kpc
A 496
(d)
1 arcmin = 52.7 h_{50}^{-1} kpc
T (keV)
R (arcmin)

Figure 1

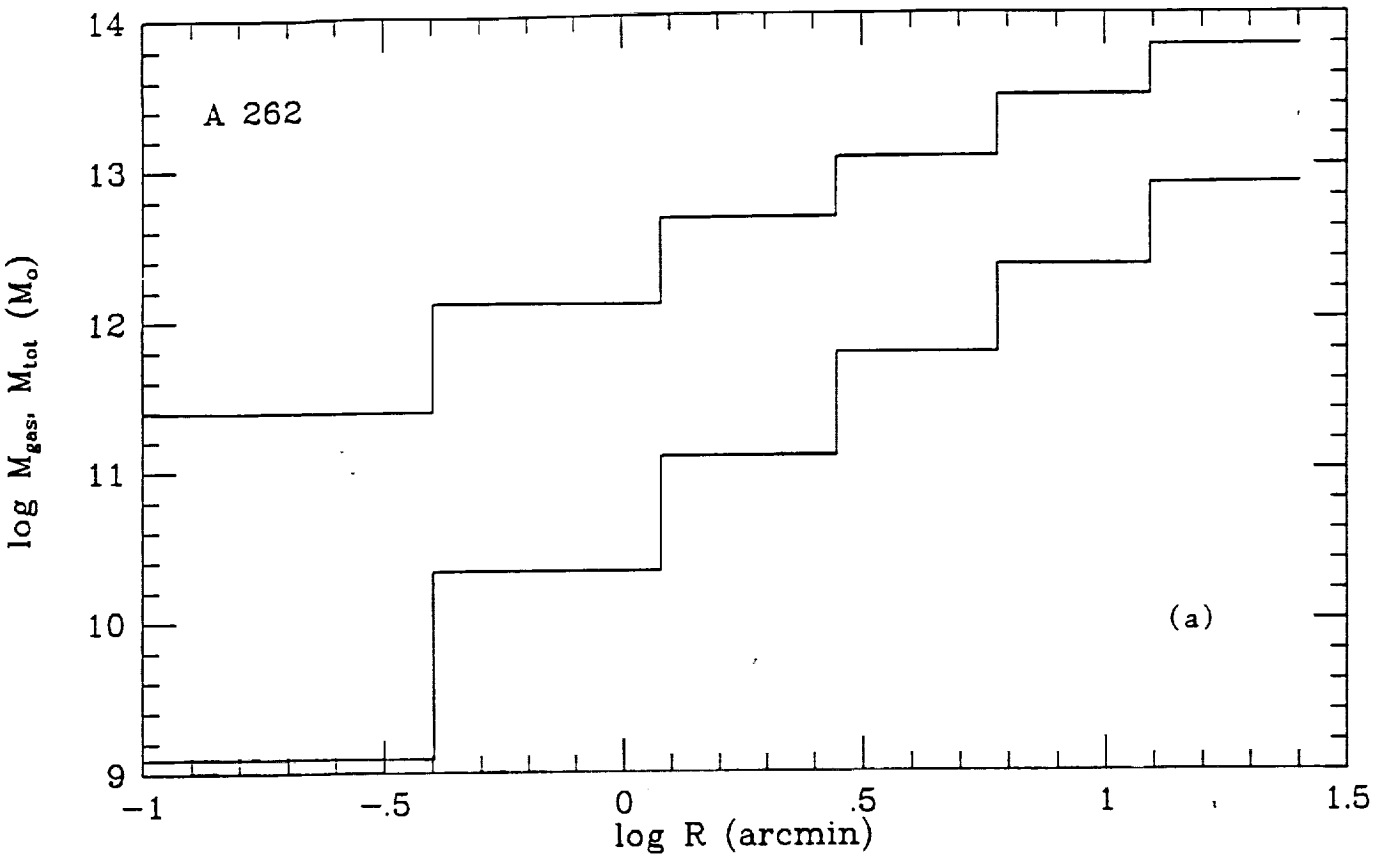
A 262
(a)
log M_{gas}, M_{tot} ($M_\odot$)
log R (arcmin)
14
13
12
11
10
9
−1
−.5
0
.5
1
1.5

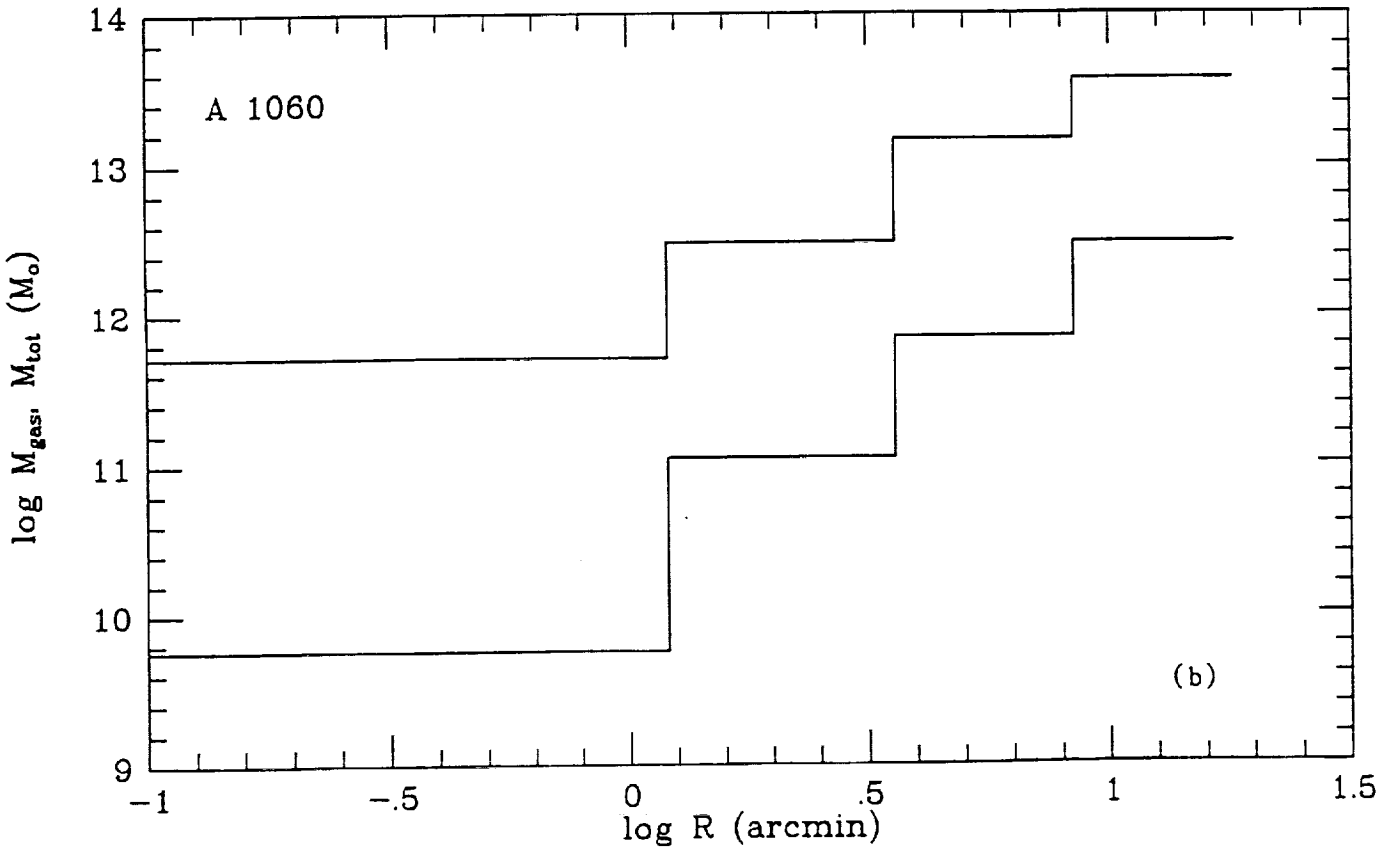
A 1060
(b)
log M_{gas}, M_{tot} ($M_\odot$)
log R (arcmin)
14
13
12
11
10
9
−1
−.5
0
.5
1
1.5

Figure 2

Figure 3

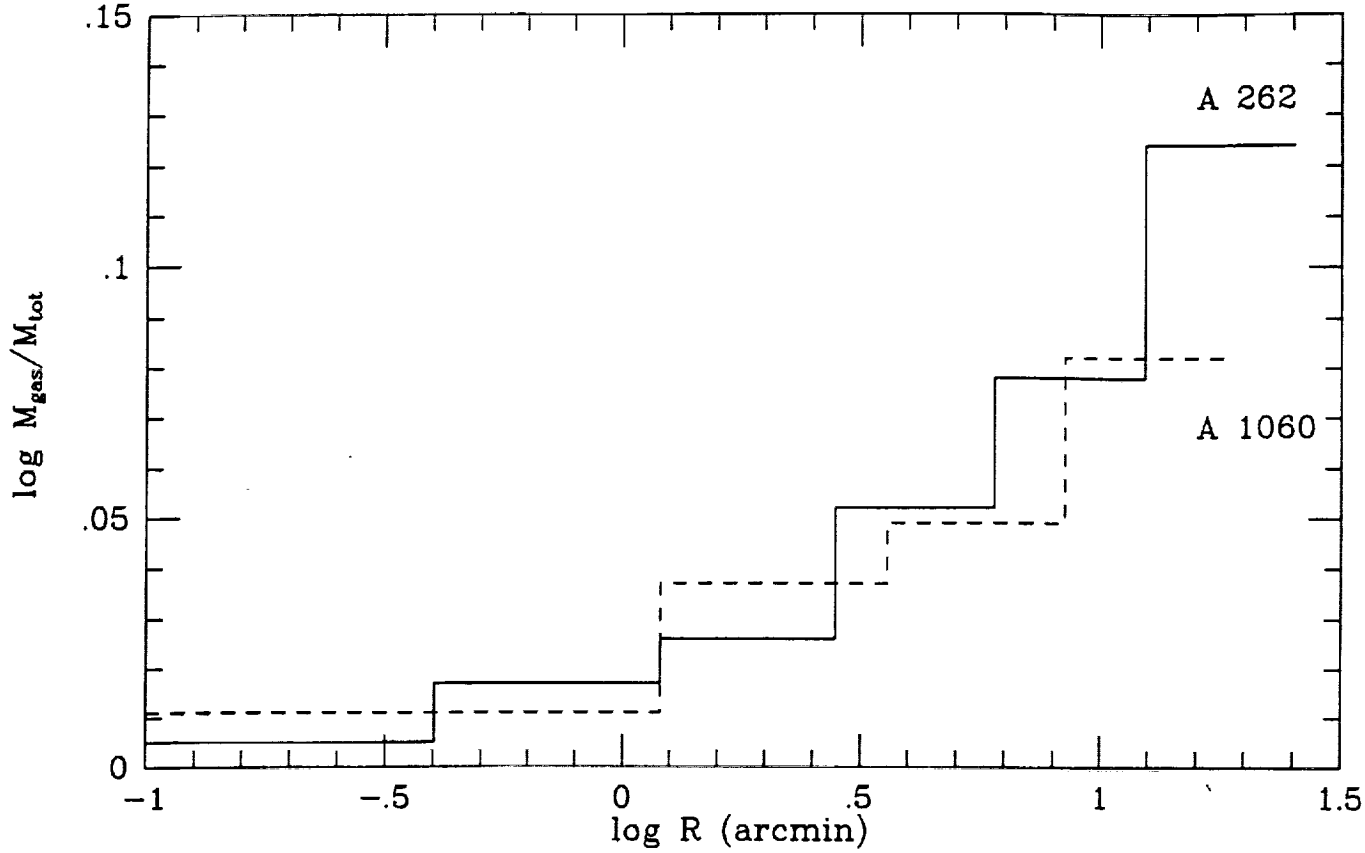

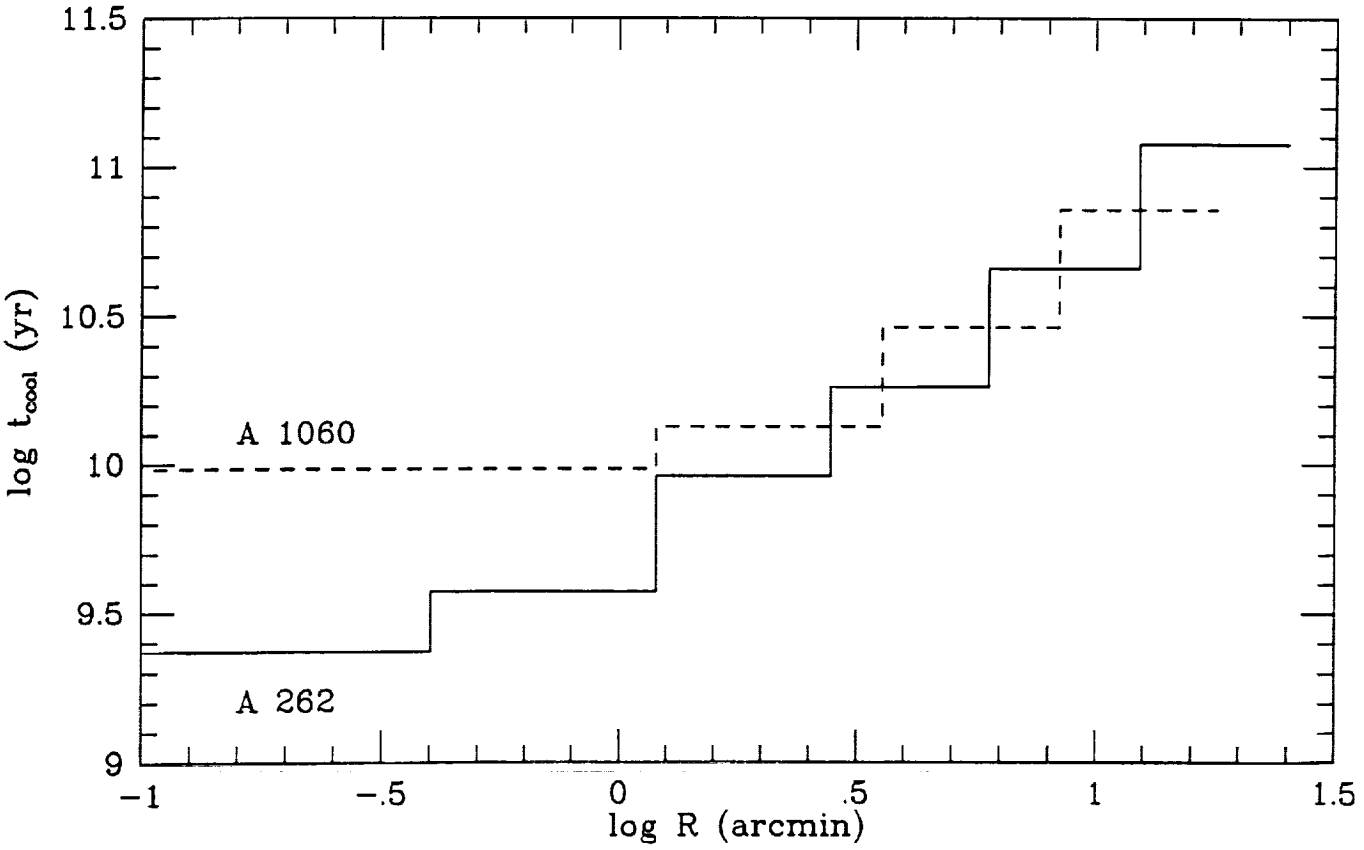

Figure 4